Radiation Oncology Articles

Radiation Oncology

2-1-2021

Therapeutic enhancement of radiation and immunomodulation by gold nanoparticles in triple negative breast cancer

Brana Janic
Henry Ford Health, bjanic1@hfhs.org

Stephen L. Brown
Henry Ford Health, Sbrown1@hfhs.org

Ryan Neff

Fangchao Liu

Guangzhao Mao

*See next page for additional authors*

Recommended Citation
Janic B, Brown SL, Neff R, Liu F, Mao G, Chen Y, Jackson L, Chetty IJ, Movsas B, and Wen N. Therapeutic enhancement of radiation and immunomodulation by gold nanoparticles in triple negative breast cancer. Cancer Biol Ther 2021.

Authors

Brana Janic, Stephen L. Brown, Ryan Neff, Fangchao Liu, Guangzhao Mao, Yalei Chen, LaToya Jackson, Indrin J. Chetty, Benjamin Movsas, and Ning Wen
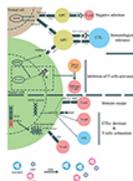
Therapeutic enhancement of radiation and immunomodulation by gold nanoparticles in triple negative breast cancer

Branislava Janic, Stephen L. Brown, Ryan Neff, Fangchao Liu, Guangzhao Mao, Yalei Chen, Latoya Jackson, Indrin J. Chetty, Benjamin Movsas & Ning Wen

Published online: 18 Jan 2021.

Submit your article to this journal

Article views: 411

View related articles

View Crossmark data

Taylor & Francis
Taylor & Francis Group

RESEARCH PAPER

OPEN ACCESS | Check for updates

Therapeutic enhancement of radiation and immunomodulation by gold nanoparticles in triple negative breast cancer

Branislava Janic [a], Stephen L. Brown[a], Ryan Neff[b], Fangchao Liu[c], Guangzhao Mao[c,d], Yalei Chen[e], Latoya Jackson[e], Indrin J. Chetty[a], Benjamin Movsas[a], and Ning Wen[a]

[a]Radiation Oncology, Henry Ford Hospital, Detroit, Michigan, USA;; [b]University of Notre Dame, South Bend, Indiana, USA; [c]Department of Chemical Engineering and Materials Science, Wayne State University, Detroit, Michigan, USA; [d]School of Chemical Engineering, Unsw Sydney, Kensington, Australia; [e]Department of Public Health Sciences, Henry Ford Hospital, Detroit, Michigan, USA

ABSTRACT

Gold nanoparticles (AuNPs) have been shown to enhance cancer radiotherapy (RT) gain by localizing the absorption of radiation energy in the tumor while sparing surrounding normal tissue from radiation toxicity. Previously, we showed that AuNPs enhanced RT induced DNA damage and cytotoxicity in MCF7 breast cancer cells. Interestingly, we found that cancer cells exhibited a size-dependent AuNPs intracellular localization (4 nm preferentially in the cytoplasm and 14 nm in the nucleus). We extended those studies to an *in vivo* model and examined the AuNPs effects on RT cytotoxicity, survival and immunomodulation of tumor microenvironment (TME) in human triple negative breast cancer (TNBC) xenograft mouse model. We also explored the significance of nanoparticle size in these AuNPs' effects. Mice treated with RT and RT plus 4 nm or 14 nm AuNPs showed a significant tumor growth delay, compared to untreated animals, while dual RT plus AuNPs treatment exhibited additive effect compared to either RT or AuNPs treatment alone. Survival log-rank test showed significant RT enhancement with 14 nm AuNP alone; however, 4 nm AuNPs did not exhibit RT enhancement. Both sizes of AuNPs enhanced RT induced immunogenic cell death (ICD) that was coupled with significant macrophage infiltration in mice pretreated with 14 nm AuNPs. These results showing significant AuNP size-dependent RT enhancement, as evident by both tumor growth delay and overall survival, reveal additional underlying immunological mechanisms and provide a platform for studying RT multimodal approaches for TNBC that may be combined with immunotherapies, enhancing their effect.

Introduction

Radiation therapy (RT) as a standard of care for more than half of all cancer patients,[1,2] exerts its cytostatic and cytotoxic effects *via* DNA damage. However, radiation ionizations are random and do not discriminate between cancer cells and surrounding normal tissue. Hence, RT efficiency is fundamentally limited by early and late side effects that profoundly affect patients' quality of life.[3] In addition, RT cytotoxicity has been a major limiting factor in maximizing deposited RT dose and a significant obstacle in cancer treatment planning.[4] Therefore, one solution to these obstacles that has been an area of active research is the enhancement of RT therapeutic ratio through developing strategies for a delivery of higher RT doses to the tumor itself, while minimizing damage to the surrounding normal tissue.[5] This can be achieved through modulating a tumor response to RT by using radiosensitizers, such as nanoparticles that increase the sensitivity of cancer cells to irradiation.[6] Particularly promising as radio-sensitizers are NPs containing metals of high atomic number (Z) due to their high absorption coefficient. The targeting of NPs to tumor tissue coupled with the high stopping power of metals compared to soft tissue increase the local radiation dose deposition. Among metal NPs, gold NPs (AuNPs) have been proposed as attractive radio-sensitizers due to the high Z of

gold. Gold has a large photoelectric cross section and a high probability of secondary electrons and associated free radicals production.[7] This photoelectric effect is most dominant at low, kilo voltage (kV) energy levels where it causes a significant increase in the absorbed radiation dose.[8,9] On the other hand, at clinically relevant x-ray energies at the megavoltage (MV) range, the dominant physical event is Compton scattering that is not expected to cause significant AuNP sensitization;[10,11] but observed RT enhancement at these energies is still significant and has been explained by a combination of physical, chemical, and biological mechanisms.[10,12,13] Radiosensitization by AuNPs remains an active area of research in the preclinical setting,[8,14–17] where experimentally measured dose enhancement was greater than predicted based on the mass attenuation coefficients, confirming that mechanisms other than physical are involved in AuNP radio-sensitization.[18] Recent studies indicated that oxidative stress in cells caused by reactive oxygen species generated by AuNPs in the absence of ionizing radiation may account for radio-sensitization *via* biological mechanisms.[11,19,20] However, most AuNP studies remain preclinical, awaiting clinical translation and biosafety confirmation.[13]

Recent research showed that beside cytostatic and cytotoxic effects, RT exhibits immunomodulatory effect on tumor

microenvironment (TME) as well, an effect that has drawn huge research interest. Radiation immunomodulation is achieved through mechanisms such as immunogenic cell death (ICD),[21,22] tumor neoantigen presentation,[23] cytokine secretion and activation and priming of host antitumor T cells.[24] Therefore, RT may have potential to convert the irradiated and damaged cancer cells into an *in situ* vaccine and to stimulate immunogenicity of tumor microenvironment, important for inducing antitumor immunity. In "immunologically cold" cancers, such as very aggressive triple negative breast cancer (TNBC), increase in tumor microenvironment immunogenicity has been associated with a better prognosis as a result of enhanced responses to chemotherapy and immunotherapy.[25]

Particularly important in the RT immunomodulation process is ICD whereby signals such as calreticulin and nuclear protein high-mobility group box-1 (HMGB-1) (a.k.a. damage-associated molecular patterns (DAMPs)) are generated.[22,26] These signals are instrumental in initiating anti-tumor immunity. DAMPs trigger dendritic cell (DC) recruitment, antigen uptake and presentation to CD8 + T cells and a consequent adaptive long-term immunity,[26] and have been explored as potential prognostic breast cancer markers.[27] However, a direct link between RT regimen and ICD induction remains elusive. It is also not clear if biological mechanisms involved in AuNP mediated RT dose enhancement include changes in RT immunomodulatory properties as well. Breast cancer (BC) models have been frequently used in exploring the effects of radiation therapeutics and recent work in syngeneic TNBC 4T1 mouse models explored RT potential in mediating immune response elements such as CD8 + T cells[28] and chemokine secretion.[29] However, very few analyzed the AuNPs as RT enhancer in TNBC MDA MB 231 model[30] and there has been no exploration on immunological effects. Since TNBC is one of the most aggressive forms of BCs with extremely low rate of survival and very limited treatment options,[31] we seek to develop strategies for improving TNBC radiation therapy outcome. In this study, we used human MDA MB 231 TNBC mouse xenograft model to investigate the potential of AuNPs to enhance radiotherapy and modulate immunological properties of TME. We used two different core sizes of AuNPs, 4 nm and 14 nm, because they are within the size range of suggested optimums for most efficient cellular uptake, accumulation and distribution within the tumors[32] and least possibility for systemic toxicity.[33] We examined the capacity of AuNPs to enhance RT effects *in vivo* in MDA MB 231 xenograft mouse model. First, we qualitatively confirmed the cellular uptake and intracellular localization of 4 and 14 nm AuNPs by transmission electron microscopy (TEM). We next showed that both 4 nm and 14 nm size AuNPs when delivered intratumorally enhanced RT effects that lead to a decrease in tumor volume, while overall increase in survival was achieved only with 14 nm AuNPs. Interestingly, AuNPs effects were accompanied by changes in the expression of immunologically relevant markers such as calreticulin and macrophage infiltration. The results of this study indicate that local intratumor delivery of AuNPs is a promising strategy for developing AuNP radio-sensitization clinical protocols. In addition, these data provide valuable information on the potential role of immunological processes in the mechanisms of AuNP mediated RT enhancements.

Results

AuNP uptake by MDA MB 231 cells

Cellular uptake of AuNPs can be achieved *via* passive translocation across the cell membrane or through active endocytosis[34] and it can be influenced by nanoparticle size, shape, surface chemistry and dose.[35] We performed a qualitative analysis of the cellular uptake of 4 nm AuNPs and 14 nm AuNPs by the MDA MB 231 breast cancer cells using TEM. Cells were incubated with 4 nm AuNP or with 14 nm AuNP for 2 h, after which cells were extensively washed to remove excess or any surface-attached nanoparticles. TEM image analysis revealed numerous high electron density-staining particles inside the cells incubated with AuNPs (Figure 1(a, Figure 1b)). In MDA MB 231 cells incubated with 4 nm AuNPs, nanoparticle clusters were detected throughout the cytoplasm with the majority of AuNPs trapped within the membranous structures/vesicles (Figure 1(a)). Most of these vesicles were located in the vicinity of nucleus (Nu), but some were found in the proximity of mitochondria (MT)
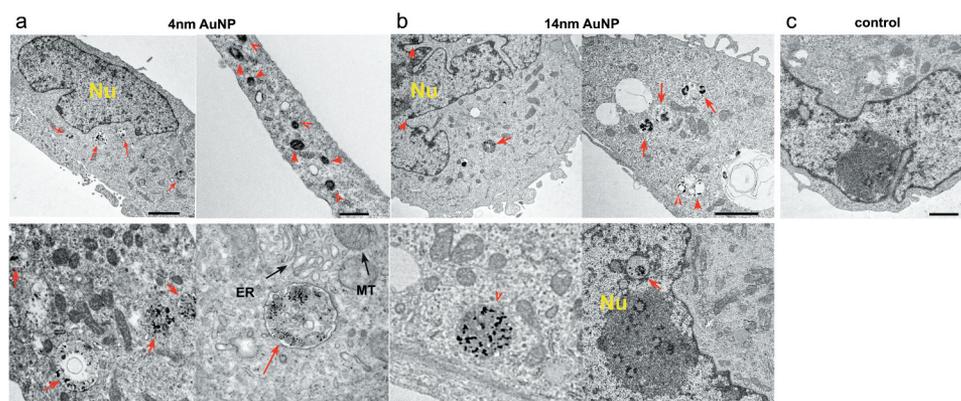
Figure 1. Cellular uptake of AuNPs by MDA-MBA 231 cells. (A) TEM images of MDA MB 231 cells exposed to 4 nm AuNPs showing the internalized high electron density-staining particles inside vesicles (red arrows). (B) TEM images of MDA MB 231 cells incubated with 14 nm AuNPs where some AuNPs were detected inside the cytoplasmic vesicles (red arrows), while portion some AuNPs were found within the nuclei (red arrows; bottom panels). (C) TEM image of MDA MB 231 cells not exposed to AuNPs (control).

and endoplasmic reticulum (ER). Magnified images of vesicles containing AuNPs are shown in the bottom panels of Figure 1 (a). Similar intracellular distribution was observed in MDA MB 231 cells incubated with 14 nm AuNPs (Figure 1(b)). However, sparse, less aggregated granules of high electron density were also observed in the nuclei, indicative of nuclear AuNP uptake, which was not observed in cells incubated with 4 nm AuNP (bottom panels, Figure 1(b)). Images of control cells that were not treated with AuNPs are shown in Figure 1(c). Altogether, TEM data demonstrated MDA MB 231 cellular uptake of AuNPs with a potential nanoparticle size-dependent differential intracellular localization. In addition, MDA MB 231 cell morphology exhibited unremarkable subcellular compartments indicating that AuNPs did not alter MDA MB 231 cell activity and metabolically active status.[36]

Therapeutic efficacy and toxicity in vivo

Treatment efficacy was measured by a percentage change in tumor volume (Figure 2). Mice treated with RT and RT plus 4 or 14 nm AuNP showed a significant tumor growth delay starting at days 7 and 4, respectively, compared to their untreated controls ($p < .05$). Mice receiving 4 or 14 nm AuNP also exhibited significant tumor growth delay in AuNP plus RT treatment group, compared to RT alone treatment ($p < .05$) that was observed on day 30 in mice receiving 4 nm AuNP and on day 19 and 23 in mice receiving 14 nm AuNP (Figure 2(a,Figure 2b)). Interestingly, 7 days post-treatment with 4 nm AuNP alone mice showed significant tumor growth delay, compared to the untreated controls. Similarly, in animals treated with 14 nm AuNP alone significant tumor growth delay, compared to the untreated controls was observed starting at day 4 and this effect was of the similar magnitude and pattern as observed in animals treated with RT alone and at day 26 the effect was the same as observed in RT + AuNP treatment group (Figure 2(a,Figure 2b)).

Systemic toxicity was evaluated by calculating the percentage of body weight loss (Figure 3). There were significant changes in body weight, but their magnitude was relatively minor, less than ± 10% throughout the course of the entire study. In animals treated with 4 nm AuNP alone, a significant difference in the percentage of body weight change (loss of weight) was observed compared to that of the control, non-treated group at days 11 and 15 and in animals treated with RT + 4 nm AuNP combination at days 4, 7, 11 and 15 compared to that of the control, non-treated group ($p < .05$)(Figure 3(a)). However, in animals treated with 14 nm AuNP alone, body weight was significantly higher at day 4,7 and 11, compared to the control, non-treated animals and compared to RT treatment group at days 4, 11, 19 and 23 ($p < .05$), indicating less toxicity in the presence of 14 nm AuNPs (Figure 3(b)).
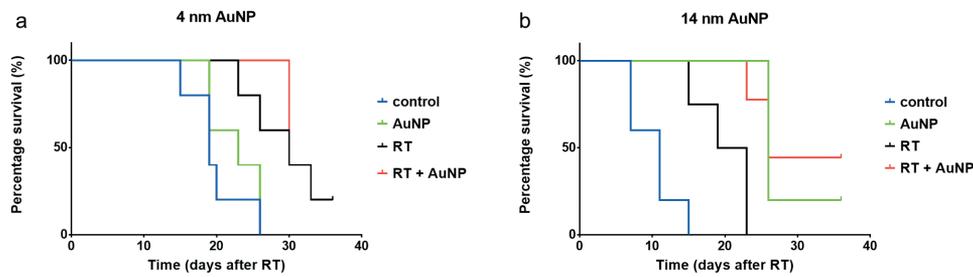
Survival analysis using log-rank (Mantel-Cox) test indicated significant survival differences among treatment groups (Figure 4 (a,b)). Further comparison revealed significant increases in survival in the RT group compared to untreated controls ($p < .005$) as well as an increase in survival of groups treated with RT + 4 nm AuNP and RT + 14 nm AuNP, compared to the control groups ($p = .0018$ and $p < .0001$, respectively, Table 1 and Table 2). Significant potentiation of RT survival effect was achieved when RT was combined with 14 nm AuNPs ($p = .0006$) (Table 2), while 4 nm AuNP was not effective. Furthermore, treatment with 14 nm AuNPs alone significantly increased the survival compared to RT
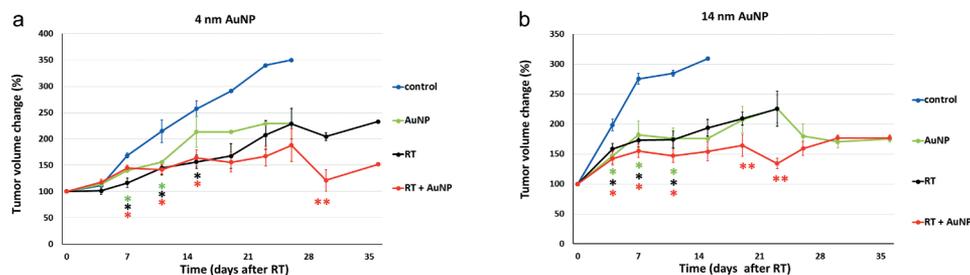
Figure 2. Effect of AuNPs on RT induced tumor growth delay. Primary tumor volumes were measured at 3–4 days intervals by calipers and calculated using the formula: $4/3\pi \times$ Length $\times$ Width $\times$ ((Length + Width)/2)/8. Percentage of tumor volume change over time in mice treated with 4 nm AuNPs (n = 5) (**A**) and 14 nm AuNPs (n = 5–9) (**B**). Data represent mean ± SEM *p < .05 compared to control; **p < .05 compared to RT alone.
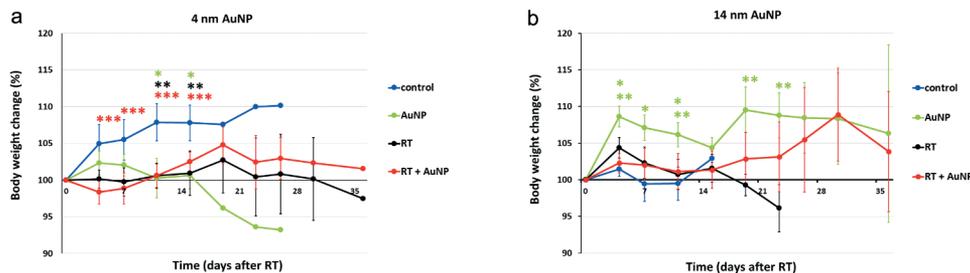
Figure 3. Effect of AuNPs and RT on body weight change. (**A**) Percentage body weight change in animals receiving 4 nm AuNP. Animals were weighed two times per week; Data represent mean ± SEM (n = 5). *p < .05 for 4 nm AuNP alone compared to control; **p < .05 for RT compared to control; ***p < .05 for RT + 4 nm AuNP compared to control (**B**) Percentage body weight change in animals receiving 14 nm AuNP. Animals were weighed two times per week; Data represent mean ± SEM (n = 5–9). *p < .05 for 4 nm AuNP alone compared to control; **p < .05 for 4 nm AuNP alone compared to RT alone.

Figure 4. Effect of AuNPs and AuNP enhanced RT on survival. Survival analysis by log rank Mantel Cox test. Compared to untreated control groups, significantly prolonged survival was achieved for the following groups: RT alone and RT + 4 nm AuNP (**A**), and RT alone, 14 nm AuNP alone and RT + 14 nm AuNP (**B**). Compared to RT alone treatment groups, significantly prolonged survival was achieved for the following groups: 14 nm AuNP alone and RT + 14 nm AuNP and (**B**).

Table 1. Survival analysis - 4nm AuNP experiments.

4 nm AuNP experiments	Comparison	95% CI of ratio	p
	RT vs control	0.4240 to 5.880	0.0142
	RT + AuNP vs control	0.4240 to 5.880	0.0018

Table 2. Survival analysis - 14nm AuNP experiments.

14 nm AuNP experiments	Comparison	95% CI of ratio	p
	RT vs control	**0.6245 to 5.836**	**0.0009**
	AuNP vs control	**0.6347 to 8.802**	**0.0019**
	RT + AuNP vs control	**0.6843 to 8.165**	**<0.0001**
	RT vs AuNP	**0.2432 to 2.682**	**0.0014**
	RT vs RT + AuNP	**0.2642 to 2.469**	**0.0006**

alone ($p = .0014$). Median survival and "n" values are shown in Table 3.

Intratumor distribution of injected AuNPs was macroscopically determined in tumor tissues collected at day 26 of the study. Analysis of harvested tumor sections revealed rather heterogeneous distribution of AuNPs within the tumor. However, 14 nm AuNPs more evenly dispersed within the tissue, while 4 nm AuNPs congregated in visible clusters (Figure 5(a,Figure 5b). Figure C shows tissue from control animals.

Table 3. Median Survival.

		control	AuNP	RT	RT + AuNP
4 nm AuNP experiments	**n**	5	5	5	5
	Median survival	19	23	30	30
14 nm AuNP experiments	**n**	5	5	8	9
	Median survival	11	26	21	26

AuNP effects on TME immunological properties

We next investigated whether the observed therapeutic effects were associated with changes in tumor microenvironment immunological properties. Collected tumor tissues were analyzed by immunohistochemistry for the expression of activated, cleaved Caspase 3, calreticulin and macrophage infiltration. These parameters were previously shown to be associated with programmed cell death and ICD.[37] Tissue staining for the cleaved Caspase 3 revealed higher percentage of positive stain in mice receiving RT alone, as well as RT + 4 nm AuNPs and RT + 14 nm AuNPs, compared to control non-treated animals ($p < .05$). However, addition of AuNPs to RT treatment did not induce significant increase in cleaved Caspase 3 expression, compared to RT treatment alone. Although the addition of 4 nm AuNP exhibited potentiation of RT effect, this increase was not statistically significant compared to RT alone. Percent of cleaved Caspase 3 positive stain in animals treated with either 4 nm AuNPs or 14 nm AuNPs was similar as observed in control, non-treated animals (Figure 6(a)). Representative digital microscopy images of cleaved Caspase 3 immunohistology staining are shown in Figure 6(b). Tissue analysis of calreticulin expression revealed increase in the percentage of positive cells in animals receiving RT alone as well as 14 nm AuNP alone ($p < .05$). In mice receiving the combination of 4 nm AuNPs + RT or 14 nm AuNPs, this effect was further significantly potentiated in comparison to the effect of RT alone ($p < .05$) (Figure 6(c)). Representative digital microscopy images of tissues stained with anti-calreticulin antibody are shown in Figure 6(d). Lastly, macrophage infiltration in tumor tissue sections were analyzed by staining for the F4/80 pan macrophage marker (Figure 6(e)). No difference was observed in animals receiving single treatment of RT, 4 nm AuNPs or 14 nm AuNPs compared to non-treated, control group of animals. However, the addition of 14 nm AuNP to RT treatment significantly increase macrophage infiltration compared to control non-treated group of animals as well as

Figure 5. Intratumoral distribution of administered AuNP. Macroscopic images of MDA MB 231 transplanted tumors excised at day 26. Tumors extracted from animals receiving 14 nm AuNP (A), 4 nm AuNPs (B) and animals that did not receive any AuNP (C).
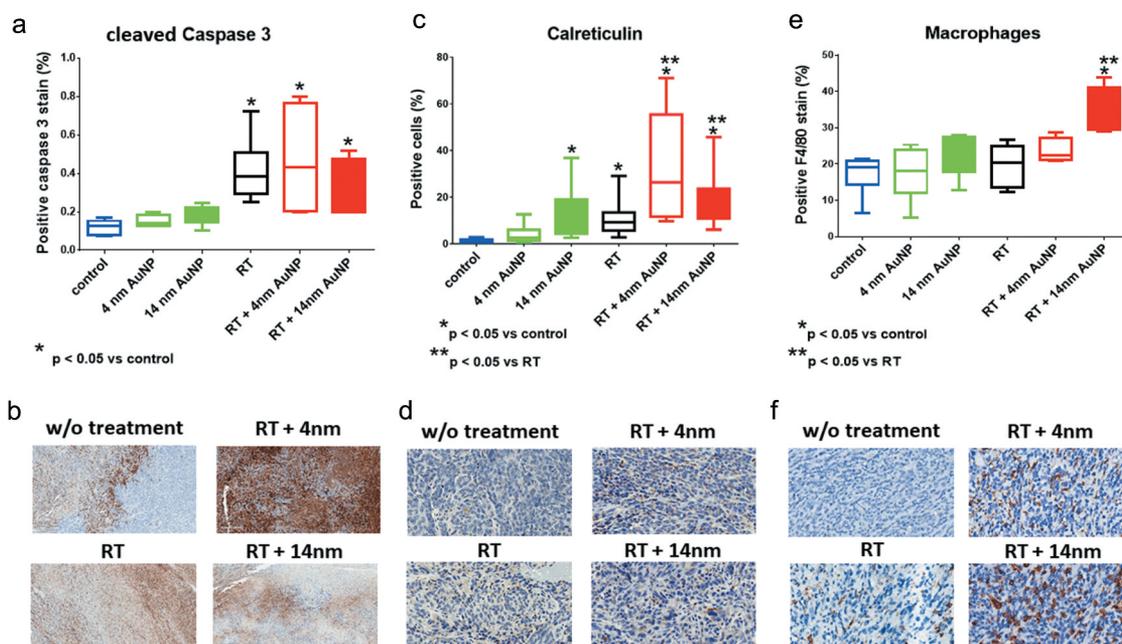
Figure 6. Effect of AuNPs and AuNP enhanced RT on tissue expression of cleaved Caspase 3, Calreticulin and macrophage infiltration. Immunohistochemistry analysis of the percentage of positive stain for cleaved Caspase 3 (**A**) and F 4/80 (**E**) and for the percentage of cells positive for Calreticulin (**C**). Digitalized tissue stains were evaluated for staining extent and intensity by QuPath software custom made application. Data expressed as mean + SEM (n = 5). *p < .05 compared to control; **p < .05 compared to RT alone. Corresponding representative images of tissue stains are shown in panels **B, D** and **F**.

compared to animals treated to RT alone. Representative digital microscopy images of F4/80 staining are shown in Figure 6(b).

Discussion

Triple negative breast cancer (TNBC) is the most aggressive BC form that accounts for 15–20% of all the BCs.[38] When diagnosed, TNBC is typically presented as a high-grade tumor with a high rate of distant metastases[39] and a very low rate of a disease-free and overall survival (<18 months).[31] Patients with TNBC have very limited treatment options that usually include chemotherapy and radiation; however, they very often fail due to developed resistance to these therapies.[40] TNBC radiation resistance in particular, was demonstrated to be linked to the slow tumor cell cycle progression that allows time for radiation induced DNA damage to be efficiently repaired.[41] Thus, the aggressive nature of TNBC coupled with a significant toxicity and suboptimal outcomes of the current therapies necessitate development of new and effective TNBC treatment strategies. We seek to develop nanoparticle-based strategies for improving TNBC radiation therapy outcome. Therefore, we investigated the capacity of AuNPs to enhance the effect of a single dose of RT in TNBC MDA MB 231 tumor model. Since TNBC outcome is greatly influenced by the ability of host immune system to develop antitumor response, we also examined AuNPs' effects on immunological properties of MDA MB 231 tumor microenvironment (TME).

Therapeutic potential of AuNPs strongly depends on nanoparticles size, shape, and functional modification. These important parameters affect nanoparticles *in vivo* circulation half-life, biodistribution, tumor uptake, and toxicity. Particularly important are the level of AuNPs cellular uptake

and intracellular localization and proximity to various organelles/compartments, since these can profoundly influence magnitude and type of cellular responses to stress, such as ionizing irradiation or AuNP itself. It has been shown that AuNPs with diameters of 10–30 nm exhibited optimal characteristics with regard to circulation half-life and intratumor accumulation and diffusion.[42] Conversely, larger nanoparticles (>50 nm) were associated with a lower uptake by tumors and probable capture by liver, while smaller nanoparticles (<10 nm) were more readily excreted by kidneys.[8,43] At the cellular level, intermediate size AuNPs (10–50 nm) were shown by most studies to exhibit the greatest uptake,[43,44] while smaller AuNPs (<5 nm) need to aggregate to be endocytosed.[43,45] On the other hand, once inside the cell smaller AuNPs generate more ROS than larger AuNPs, due to larger surface area to volume ratios.[46,47] In addition to AuNP size, surface modification also has an important role in AuNPs therapeutic potential. Surface coating with PEG has been commonly used to stabilize and prolong AuNPs' circulation half-life and intratumor distribution,[42,48] however the same PEG coating was also shown to decrease the level of AuNPs cellular uptake and the production of ROS needed for AuNPs radio-sensitization to take place.[18,49] Considering all these factors we opted to use spherical AuNPs of 4 nm and 14 nm in size, surface capped by a monolayer of mercaptosuccinic acid (MSA). Our previous work using identical nanoparticle preparations demonstrated no cytotoxicity *in vitro* and no toxicity *in vivo*.[15,50–52] In agreement with our previous report on MCF-7 breast cancer cells,[15] in this study both 4 nm and 14 nm size AuNPs were successfully taken up by MDA MB 231 cells without changes in their cellular morphology. Both size AuNPs were found inside the cytoplasmic vesicles (endosomes and lysosomes) that were

detected in the vicinity of mitochondria, endoplasmic reticulum and nuclei. It is of note that 14 nm AuNPs were found in the nuclei as well. It was previously proposed that nuclear import *via* the nuclear pore complex is expected for nanoparticles of less than 30 nm in diameter,[53] while particles smaller than 9 nm enter the nuclei by passive diffusion.[54] However, in our current study using MDA MB 231 cells and our previously published work in MCF-7 cells, 4 nm AuNPs were found in the cytoplasm only with no presence in the nuclei. As mentioned, AuNPs smaller than 5 nm in size need to aggregate to be endocytosed,[43,45] therefore, it is possible that aggregation of 4 nm AuNPs resulted in larger complexes that were incompatible with nuclear transport. However, the actual mechanisms explaining the observed nuclear 14 nm AuNP localization remain unresolved. Similar to our findings, nuclear AuNPs localization was reported in MCF-7 after endocytosis of 15.6 nm size PEG-coated AuNPs.[55] Then again, in MDA MB cell lines previous work implicates various factors, such as sedimentation rate, diffusion speed, irregular morphology, and concentration of aggregates playing a role in AuNPs' cellular uptake and trafficking.[32,56] In summary, an explanation of the mechanisms for the observed nuclear 14 nm AuNP localization require further investigation. Our data shown here agree with previous, limited number of studies exploring AuNPs' therapeutic potential in human breast cancer cell lines. These studies showed cellular uptake and localization within the endosome/lysosome compartment for PEG coated and functionalized small (5 nm) and large (100 nm) AuNPs in MDA MB 231 cells[30,57] and for 10.8 nm "naked" and 15.6 nm PEG-modified AuNPs in MCF-7 cell line.[9,55] As shown by previous work, the level of cellular uptake and intracellular localization have significant impact on AuNP induced oxidative stress and enhancement of radio sensitization.[19,44] Particular intracellular AuNPs localization as well as proximity to various organelles and compartments may govern the type and magnitude of cellular responses to stressors such as ionizing irradiation or AuNPs alone. For a maximum DNA damage to take place, AuNPs nuclear localization is desired where close proximity to DNA would maximize the effectiveness of photoelectric effect at low radiation energies as well as the damaging effect by AuNP's ROS production and induced chemical sensitization.[3,58] On the other hand, sufficient evidence demonstrated that nuclear localization is not necessary for AuNPs radio sensitization and that sole close proximity to crucial cellular components may facilitate stress and damage by ROS and short-range low energy electrons produced by AuNP alone or under low radiation energy, respectively.[17,18] Organelles or compartments undergoing stress elicit signaling cascade for programmed cell death execution. However, the type of the cell death initiated (apoptosis vs. ICD) will depend on what organelle or cell compartment death signal originates from and will affects the magnitude of overall tissue damage and inflammatory and immune response.[37,59] Therefore, our findings on different intracellular localization indicate that nanoparticle size-dependent differences in AuNPs mediated RT enhancement observed in *in vivo* experiments may be due to a difference in observed intracellular localization between 4 nm and 14 nm AuNPs that dictated different magnitude and

temporal occurrence of DNA damage, mitochondrial and ER stress as underlying mechanisms of cell death initiation.

Radio sensitization by AuNPs have been evaluated in numerous *in vivo* studies. However, many critical parameters, such as tumor model, AuNPs administration dose and route, RT dose and dosing schedule of AuNPs and RT, varied across these studies with still no consensus on optimal condition for the best therapeutic outcome. Various tumor models have been used to investigate AuNP radiosensitizing potential using a broad range of AuNP doses, with total intratumor AuNPs levels varying between 0.25 ug to 70 mg of gold per gram of tumor.[8,60–67] In the current study we used 100 ug per tumor that resulted in detectable therapeutic effect with 14 nm AuNP alone and enhancement of RT effect with both 4 nm and 14 nm AuNPs. Previous studies indicated that systemic, intravenous administration of AuNPs delivers less than 7% of injected dose to the tumor site due to their capture by organs such as liver and spleen, which may cause systemic toxicity.[68,69] To avoid AuNPs entrapment by liver and spleen and potential systemic toxicity, and to maximize AuNPs accumulation at the tumor site,[30,60] the current study employed direct intratumor AuNPs injection. To ensure nanoparticles availability within the tumor as well as their cellular uptake, AuNPs were administered 24 h prior to irradiation. Most of the reported *in vivo* work evaluating AuNPs radiosensitization effects utilized a single administration of a high irradiation dose (5–50 Gy) since a detectable therapeutic response is expected to be observed within that range in a majority of available tumor models.[14,18,60,70] Various reasonings behind the dose of choice have been provided; however, a clear mechanistic justification and consensus on it has yet to be offered. Studies by Hainfeld et al. suggested that at low doses AuNPs may not exhibit therapeutic improvement, while high doses may elicit toxicity.[70] Thus, an effective dose for assessing AuNPs potential to enhance RT would be below the toxicity threshold but high enough to induce therapeutic response. Based on our previous work and our experience with different tumor models we opted to use a single high RT dose of 15 Gy.[71] In a clinical setting administration of a single high dose of RT in BC patients was explored mainly as a preoperative procedure.[72,73] However, most clinical BC protocols consist of fractionated regimens of lower RT doses, indicating the need for future exploration of AuNPs potential using fractionated low RT doses, also suggested to provide superior conditions for AuNP radio sensitization.[65] On the other hand, breakthroughs with stereotactic ablative body radiotherapy (SABR) showing that precisely administered high RT doses in a small number of fractions doubled median survival for oligometastatic disease[74] and significantly increased the response rate to cancer immunotherapy,[75] open the possibility for a clinical AuNPs application at high RT doses as well. Our experiments reported here based on the use of a single high RT dose delivered significant radiation enhancement effect with 4 nm and 14 nm AuNPs. In the absence of radiation both 4 nm and 14 nm AuNPs induced significant tumor growth delay compared to that of the untreated control group. This effect was equivalent to RT alone treatment in mice receiving 4 nm AuNPs, and to RT + AuNPs in mice receiving 14 nm AuNPs. However, treatments

with 4 nm AuNPs alone or in combination with RT exhibited an observable, though not significant, systemic toxicity, which was absent in animals receiving 14 nm AuNP. Since small size AuNPs previously demonstrated increased potential in ROS production even in the absence of radiation,[3,46] it is possible that intra and extracellular pathways triggered by this property played a role in the observed toxicity. Significant radiation enhancement evaluated by survival was achieved with 14 nm AuNPs alone or in combination with RT. At the same time, 4 nm AuNPs did not deliver overall survival significance. Failure of 4 nm AuNPs to show statistically significant RT enhancement measured by overall survival may be due to a heterogeneous distribution of AuNPs within the tumor volume, as opposed to more homogenous distribution of 14 nm AuNPs, as observed on macroscopic cross sections of tumor tissues. Previously, this limited and unequal tumor penetration has been observed often with intratumor injections and it is most likely due to nanoparticle aggregation[30,60] that may also impact intracellular uptake and may explain the observed lack of nuclear entrance of 4 nm AuNPs. Similar to our results, the study by Cui et al. using MDA MB 231 xenografts in mice showed that small, 7 nm RME-PEG-AuNPs failed to confer significant RT enhancement using an intratumor injection of 0.5 mg of AuNP,[30] despite the utilization of RME targeted AuNPs delivery and fractionated 3×4 Gy RT regimen that were likely to enhance AuNPs effects. Since with heterogenous intratumor distribution some AuNPs most likely remain in extracellular matrix, it is possible that we only observed a trend in RT enhancement with smaller size AuNPs because AuNPs that reside outside of the cells were less effective.[19] However, further studies are needed to evaluate and confirm the effect of AuNPs size and modifications on intratumor distribution. Consistent with our observation, Chattopadhyay et al. demonstrated using similar *in vivo* TNBC xenograft model that intratumor injection of 30 nm HER-2 tagged AuNPs delivered significant enhancement of a single 11 Gy RT dose effect as measured by tumor growth delay, without detecting any systemic toxicity.[60] However, it is important to note that their experimental design differed from our study in that we used nonmodified AuNPs and eight times smaller AuNPs dose (0.8 mg/tumor vs. 0.1 mg/tumor). In addition, a scarcity of AuNPs RT enhancement studies using TNBC models and utilized diverse experimental conditions, challenge a direct comparison of results across studies.

Classical radiobiology defines mitotic cell death as a loss of replicative capacity that is determined by clonogenic assays.[76] Over the last decade, other RT induced cell death have been identified. For example, ICD, as a form of RT-induced regulated cell death (RCD), has emerged as an entity separate from other immunologically silent RCDs or apoptosis and has been implicated to play a role in governing disease progression and outcome, partially through affecting host antitumor immune response.[59] Despite its inherent immunological limitations, immunodeficient mouse model does allow for an assessment of tumor cells ICD and the host macrophage immune response.[77,78] We examined ICD by evaluating the levels of damage-associated molecular patterns (DAMPs) molecule calreticulin, an ER chaperone that is translocated to the cell surface in response to stress in a process considered to be a pre-apoptotic or pre-ICD event[37,59,79] and it may be initiated by AuNP induced ER stress even without RT.[10] Calreticulin, as well as other DAMPs, activate phagocytic and the antigen-presenting cells of an innate immune response, such as macrophages and dendritic cells and possibly drive adaptive antitumor immunity.[37] In addition to calreticulin, we evaluated the level of cleaved Caspase 3 as well, as a mean to assess total levels of RT induced apoptosis. Our findings revealed that both 4 nm and 14 nm AuNPs delivered significant enhancement of RT effect at the level of calreticulin expression. Interestingly, 14 nm AuNPs alone significantly increased calreticulin expression as well. On the other hand, the levels of RT-induced activated Caspase 3 were not enhanced by addition of either size AuNPs to RT. It is considered that RDC involving Caspase-3 activation is generally not immunogenic[80] and under our experimental condition most likely entail mitochondrial apoptotic pathway that is activated by radiation-induced DNA damage.[81] Since post irradiation DNA damage seemed to be directly linked to intracellular AuNPs presence and physical effects at the time of irradiation,[82] this mechanism may partially be responsible for the observed RT enhancement in tumor growth delay after addition of 4 nm and 14 nm AuNP. However, onset of the tumor growth delay enhancement with 14 nm AuNP was detected earlier than with the addition of 4 nm AuNP and the effect of AuNP alone was greater with 14 nm AuNPs compared to 4 nm AuNPs. Together with the observation that 4 nm AuNP did not enhance RT-induced survival, it is probable that effects of 14 nm AuNPs involve additional, cell death mechanisms. The increase in calreticulin expression and related ICD may partially account for the effect of 14 nm AuNP alone, but it does not support the differences between 4 nm and 14 nm RT therapeutic enhancements. Calreticulin acts on CD91 receptors on phagocytic cells to attract, promote and activate phagocytosis of dying cells.[59] However, corresponding data on macrophage infiltration demonstrated significant increase only in group receiving RT + 14 nm AuNP. In addition to calreticulin signaling, macrophages can response to ICD by interacting with other DAMPs such as nuclear chromatin-binding protein HMGB1 and ATP through engagement of their TLR4 and purinergic receptors, respectively.[83] Therefore, our calreticulin data may not accurately represent the post-treatment ICD levels. Since the DNA damage is a most prominent RT and AuNP enhanced RT effect, it is possible that nanoparticle size differential effect on ICD may be detected by differences in HMGB1 nuclear protein and will necessitate further investigation. In addition, the complexity of immunological cascade triggered by ICD in response to RT and its enhancement by AuNPs supersedes the investigative capacity of xenograft nude mouse model used here and will require immunocompetent environment to further analyze antigen-presenting and T cell response components.

In summary, here we demonstrated *in vivo* significant RT enhancement that was achieved by intratumor AuNPs administration, evident by both tumor growth delay and overall survival. These effects were nanoparticle size-dependent with 14 nm AuNPs delivering therapeutic enhancement. We show, that underlying mechanism in addition to cytotoxicity involve immunological changes as well. Further dissection of these immunological properties will be valuable in understanding

mechanisms of AuNPs driven events in TNBC that may be relevant in developing multimodal radio therapies that may include radiosensitizers as well as immunotherapy. In addition, experimental platform used in this work can be applied as a model for studying AuNPs mechanisms in cancer types other than TNBC.

Materials and methods

Mice

Seven to 8-week old athymic nude NCRNU f sp/sp (CrTac: NCr-*Foxn1^nu*) mice were purchased from Taconic Biosciences, and maintained in the AAALAC approved animal facility of the institutional Bioresources division. Mice were kept under pathogen-free conditions. Animal experiments were performed according to the protocol approved by Institutional Animal Care and Use Committee, IACUC # 1648.

Cell line and reagents

Human breast cancer MDA MB 231 cells were purchased from American Type Culture Collection (ATCC) (Manassas, VA). Cells were cultured in DMEM supplemented with 10% fetal bovine serum, 2 mmol/L L-glutamine, 100 U/ml penicillin, 100 ug/ml streptomycin, all purchased from Invitrogen/Thermo Fisher Corporation. Cells were maintained in a tissue culture incubator at 37°C with 5% CO_2. Cells were passaged every 3–4 days and cultured to limited passage and implanted while at the exponential phase of growth.

Gold nanoparticle (AuNP) synthesis and characterization

Gold nanoparticles were synthesized according to our previously published method.[15] Briefly, materials used for synthesis were as follows: Gold (III) chloride trihydrate ($HAuCl_4$ · $3H_2O$, 99% metal trace), sodium citrate tribasic dehydrate (≥99%), mercaptosuccinic acid (MSA, 97%), and sodium borohydride ($NaBH_4$, 98%) (all from Sigma-Aldrich) and sodium hydroxide (NaOH, 98%) (Fisher Scientific). Synthesis of MSA coated AuNP with diameter of 4 nm (AuNP4) started with a 250 ml scale reaction involving a mixture of 0.25×10^{-3} M $HAuCl_4$ · $3H_2O$ and 0.25×10^{-3} M tri-sodium citrate in deionized water, vigorously stirred at room temperature. Addition of 7.5 mL ice cold 0.1 M $NaBH_4$ solution changed the color of the solution into wine-red. After 30 min of stirring, pH was adjusted to 11 and 25 mg of MSA was added. To ensure complete ligand exchange the solution was continuously stirred for overnight. The solution was then purified and concentrated by centrifugation, using MW 10 K Millipore Amicon columns, followed by 3 washes with deionized water to remove impurities and reagents carried over from the synthesis. The final concentration in deionized sterile water was 2 mg/ml. MSA-coated AuNP with diameter of 14 nm (AuNP14) was synthesized following the Turkevich method.[84–86] In a typical 250 ml scale reaction, 0.25×10^{-3} M $HAuCl_4$ · $3H_2O$ was dissolved in deionized water and then heated to boil under vigorous stirring. Preheated 87.5 mg of trisodium citrate dissolved in 15 mL deionized water was then added. After the

color changed to wine-red, heating was continued for 25 min while stirring. Solution was then cooled down; the pH was adjusted to 11 and 25 mg of MSA added. Solution was then stirred overnight to ensure the complete ligand exchange after which it was purified and concentrated to the final concentration of 2 mg/ml using the same steps as for 4 nm AuNP. Upon completion of AuNPs synthesis, NPs were analyzed using JEOL JEM-2010 Transmission Electron Microscope (TEM) at the voltage of 200kV and current of 109 mA. Energy dispersive x-ray analysis (EDXA) spectrum was acquired on EDAX PV9756/70 ME EDS system attached to the TEM. Dynamic light scattering (DLS) and zeta potential measurements were performed using a Malvern Nano-ZS. The same AuNP preparation was previously used in *in vitro* and[15,50] and *in vivo* conditions with no associated toxicity[51,52].

Cell exposure to AuNPs

Twenty four hours prior to the exposure to AuNPs, MDA MB 231 cells were plated in 6 well cell culture dishes with total of $3–5 \times 10^5$ cells per well. Cells were cultured o/n in a tissue culture incubator at 37°C with 5% CO_2. The next day cell were treated for 2 h with either 4 or 14 nm AuNPs in a complete growth media. Fifty μl of AuNPs at the concentration of 2 mg/ml was added to the 1 ml of growth media with a final concentration of 100 ug/ml. Expressed as particles per ml the final concentration for the 4 nm AuNPs was 3.12×10^{13} particles/ml, while for the 14 nm AuNP the concentration was 7.2×10^{11} particles/ml.

Analysis of AuNP cellular uptake by transmission electron microscopy (TEM)

A total of 5×10^5 cells were plated in 6 well cell culture plates and cultured 24 h. Cells were then exposed for 3 h to AuNPs. Four nm size AuNPs were added at the concentrations of 3.12×10^{13} p/ml, while 14 nm size AuNPs were used at 7.2×10^{11} p/ml. Following exposure to AuNPs, cells were washed twice in 1x phosphate-buffered saline (PBS), and prepared for TEM as previously described.[50] In brief, cells were fixed in in 2.5% glutaraldehyde in 0.1 M Phosphate Buffer, pH 7.4 (Electron Microscopy Sciences, Hatfield, PA) for 1 h at room temperature. Cells were then scraped of the plates, centrifuged at a low speed and suspended in 2.5% glutaraldehyde. Samples were further processed at the Michigan State University (MSU) Center for Advanced Microscopy by postfixation in 1% osmium tetroxide, rinsing in distilled water, and dehydration through a graded series of acetone. At the end, samples were embedded in epoxy resin and cut into 70 nm sections that were then analyzed and photographed by JEOL 100CXII electron microscope.

Tumor implantation and treatment

For implantation, 2×10^6 of MDA MB 231 cells were suspended in 100 ul of sterile saline and were injected intramuscularly into the right flank of nude mice. Tumors were measured at 3–4 days intervals by determining perpendicular tumor diameters using external caliper and tumor volumes

were calculated using the following formula: 4⁄3π x Length x Width x ((Length + Width)/2)/8. Two weeks later, when tumors were palpable and grew to the average volume of 433 mm³, mice were randomly assigned to different treatment groups as described. First, animals received intratumor injection of 4 or 14 nm AuNPs at the concentration of 2 mg/ml. To minimize the leakage of the injected volume, AuNP were administered *via* multiple different injection sites (typically, four) to a total volume of 50 μl. Twenty-four hours after receiving AuNPs, mice were irradiated with 15 Gy dose at 160kV using an x-ray source (Faxitron small animal irradiator). Radiotherapy was administered as previously described.[71] Briefly, mice were anesthetized with the mixture of Ketamine (200 mg/kg) and Xylazine (20 mg/kg) *via* i.p. injection. Mice were positioned on a plexiglas tray, their entire bodies protected by lead shield except for the area of the tumor to be irradiated. Radio sensitization effect was assessed by determining tumor growth delay and animal survival. Tumor growth was evaluated every 3–4 days until day 36 as described above. All animals were euthanized by day 36 and the tumors excised and prepared for immunohistochemistry analysis.

Immunohistochemistry analysis

Harvested tumor tissue collected at day 15 underwent immunohistochemistry analysis. Tissues were processed routinely for 7 hours through formalin, graded ethanol alcohol, xylene and paraffin, using a VIP Tissue Tek automated tissue processor. The FFPE blocks were sectioned at 4 μm on a Microm Manual Microtome, using low profile disposable blades. The sections were mounted on Autofrost IHC slides (Fisher Scientific) to ensure the sections adhered to the slide during staining. The sections were left to dry on a drying rack overnight and placed in the 60°C incubation oven for 1 h. The slides were deparaffinized with xylene and rehydrated through a series of descending alcohols to water. The tissue slides underwent 20 min incubation with Envision FLEX (Agilent) low pH target retrieval solution in a Dako PT Linker at 97°C. The slides were placed on the Dako Autostainer Link and the following sequence was followed: The slides were blocked with Peroxidaze 1 (PX968H, Biocare Medical) for 5 min. The following primary antibodies and dilutions were used: anti-Calreticulin, 1:15000 for 20 min (Sino Biological, 13539-T60), anti-cleaved Caspase 3, 1:250 for 20 min (Cell Signaling, 9579S) and anti- F4/80 antibody, 1:500 dilution (Cell Signaling, 70076). The slides were then incubated for 30 min with Envision FLEX HRP (K8004-Agilent) mixed with XM Factor (XMF963C, Biocare Medical), and 10 min in Envision FLEX DAB (K8000, Agilent). Slides were then counterstained with Hematoxylin (K8008, Agilent) for 5 min, dehydrated through a series of alcohols, cleared in xylene and cover slipped with nonaqueous mounting medium. Images were captured by using Leica Aperio CS2 slide scanner. The positive cells stained brown. The slides were examined under a light microscope, and representative digital images were taken from a minimum of 3 slides from each animal. Digitalized tissue stains were evaluated for staining extent and intensity by QuPath software[87] custom made application. The staining extent is quantified as the number of positive pixels divided by the total number of tissue pixels, where the positive pixels are defined as pixels with positive staining optical density (OD) above threshold of 0.25. The staining intensity was presented by the average positive stain OD that was used as a measurement of the biomarker expression.

Statistical analysis

Experiments using 4 and 14 nm AuNP were performed separately, each including their own internal controls. The change of tumor volume (TV) after treatment was normalized as percentage of the initial TV (POITV) before treatment (day 0). POITV was measured at indicated time intervals. The change in the body weight after treatment was normalized as percentage of the initial body weight before treatment (day 0). Tumor volume change and body weight change data were analyzed using unpaired Student's t-test, with a statistical significance considered at the $p < .05$ level. For 4 nm AuNP experiments, n = 5 and for 14 nm AuNP, n = 5–9, as indicated in Table 3. Survival time analysis was performed by Kaplan Meier log-rank test followed by Gehan-Breslow-Wilcoxon test for differences in survival between two treatment groups. For immunohistochemistry analysis, tissues harvested from 3 animals per group that were sacrificed at day 15 were analyzed. For each mouse, 3 histology slides and 5 fields per slide were analyzed. The quantified average staining OD and staining percentage or percent of positive cells was used as an immune biomarker expression measurement. One-way ANOVA examined the expression difference across treatments. Analysis was performed using GraphPad Prism6 (San Diego, CA). Significance was set at the p value of 0.05.

ORCID

Branislava Janic http://orcid.org/0000-0002-0792-8288

References

1. Delaney G, Jacob S, Featherstone C, Barton M. The role of radiotherapy in cancer treatment: estimating optimal utilization from a review of evidence-based clinical guidelines. Cancer. 2005;104(6):1129–1137. doi:10.1002/cncr.21324.
2. Atun R, Jaffray DA, Barton MB, Bray F, Baumann M, Vikram B, Hanna TP, Knaul FM, Lievens Y, Lui TYM, et al. Expanding global

access to radiotherapy. Lancet Oncol. 2015;16(10):1153–1186. doi:10.1016/S1470-2045(15)00222-3.

3. Rosa S, Connolly C, Schettino G, Butterworth KT, Prise KM. Biological mechanisms of gold nanoparticle radiosensitization. Cancer Nanotechnol. 2017;8(1):2. doi:10.1186/s12645-017-0026-0.

4. Bentzen SM. Preventing or reducing late side effects of radiation therapy: radiobiology meets molecular pathology. Nat Rev Cancer. 2006;6(9):702–713. doi:10.1038/nrc1950.

5. Wolff D, Stieler F, Welzel G, Lorenz F, Abo-Madyan Y, Mai S, Herskind C, Polednik M, Steil V, Wenz F, et al. Volumetric modulated arc therapy (VMAT) vs. serial tomotherapy, step-and-shoot IMRT and 3D-conformal RT for treatment of prostate cancer. Radiotherapy Oncol. 2009;93(2):226–233. doi:10.1016/j.radonc.2009.08.011.

6. Linam J, Yang LX. Recent developments in radiosensitization. Anticancer Res. 2015;35(5):2479–2485.

7. He C, Chow JCL. Gold nanoparticle DNA damage in radiotherapy: A Monte Carlo study. Vol. 3. AIMS Bioengineering: AIMS Bioengineering; 2016.

8. Hainfeld JF, Slatkin DN, Smilowitz HM. The use of gold nanoparticles to enhance radiotherapy in mice. Phys Med Biol. 2004;49(18):N309–315. doi:10.1088/0031-9155/49/18/N03.

9. Kong T, Zeng J, Wang X, Yang X, Yang J, McQuarrie S, McEwan A, Roa W, Chen J, Xing JZ, et al. Enhancement of radiation cytotoxicity in breast-cancer cells by localized attachment of gold nanoparticles. Small (Weinheim an Der Bergstrasse, Germany). 2008;4(9):1537–1543. doi:10.1002/smll.200700794.

10. Butterworth KT, McMahon SJ, Taggart LE, Prise KM. Radiosensitization by gold nanoparticles: effective at megavoltage energies and potential role of oxidative stress. Transl Cancer Res. 2013;2(4):269–279.

11. Butterworth KT, McMahon SJ, Currell FJ, Prise KM. Physical basis and biological mechanisms of gold nanoparticle radiosensitization. Nanoscale. 2012;4(16):4830–4838. doi:10.1039/c2nr31227a.

12. Jeremic B, Aguerri AR, Filipovic N. Radiosensitization by gold nanoparticles. Clin Transl Oncol. 2013;15(8):593–601. doi:10.1007/s12094-013-1003-7.

13. Schuemann J, Berbeco R, Chithrani DB, Cho SH, Kumar R, McMahon SJ, Sridhar S, Krishnan S. Roadmap to clinical use of gold nanoparticles for radiation sensitization. Int J Radiat Oncol Biol Phys. 2016;94(1):189–205. doi:10.1016/j.ijrobp.2015.09.032.

14. Hainfeld JF, Dilmanian FA, Zhong Z, Slatkin DN, Kalef-Ezra JA, Smilowitz HM. Gold nanoparticles enhance the radiation therapy of a murine squamous cell carcinoma. Phys Med Biol. 2010;55(11):3045–3059. doi:10.1088/0031-9155/55/11/004.

15. Janic B, Liu F, Bobbitt K, L Brown S, J Chetty I, Mao G, Movsas B, Wen N. Cellular uptake and radio-sensitization effect of small gold nanoparticles in MCF-7 breast cancer cells. J Nanomed Nanotechnol. 2018;9(3):3. doi:10.4172/2157-7439.1000499.

16. Luo D, Wang X, Zeng S, Ramamurthy G, Burda C, Basilion JP. Targeted gold nanocluster-enhanced radiotherapy of prostate cancer. Small (Weinheim an Der Bergstrasse, Germany). 2019;15(34):e1900968. doi:10.1002/smll.201900968.

17. Chithrani DB, Jelveh S, Jalali F, van Prooijen M, Allen C, Bristow RG, Hill RP, Jaffray DA. Gold nanoparticles as radiation sensitizers in cancer therapy. Radiat Res. 2010;173(6):719–728. doi:10.1667/RR1984.1.

18. Cui L, Her S, Borst GR, Bristow RG, Jaffray DA, Allen C. Radiosensitization by gold nanoparticles: will they ever make it to the clinic? Radiotherapy Oncol. 2017;124(3):344–356. doi:10.1016/j.radonc.2017.07.007.

19. Cui L, Tse K, Zahedi P, Harding SM, Zafarana G, Jaffray DA, Bristow RG, Allen C. Hypoxia and cellular localization influence the radiosensitizing effect of gold nanoparticles (AuNPs) in breast cancer cells. Radiat Res. 2014;182(5):475–488. doi:10.1667/RR13642.1.

20. Taggart LE, McMahon SJ, Currell FJ, Prise KM, Butterworth KT. The role of mitochondrial function in gold nanoparticle mediated radiosensitisation. Cancer Nanotechnol. 2014;5(1):5. doi:10.1186/s12645-014-0005-7.

21. Galluzzi L, Buque A, Kepp O, Zitvogel L, Kroemer G. Immunogenic cell death in cancer and infectious disease. Nat Rev Immunol. 2017;17(2):97–111. doi:10.1038/nri.2016.107.

22. Demaria S, Golden EB, Formenti SC. Role of Local Radiation Therapy in Cancer Immunotherapy. JAMA oncol. 2015;1(9):1325–1332. doi:10.1001/jamaoncol.2015.2756.

23. Reits EA, Hodge JW, Herberts CA, Groothuis TA, Chakraborty M, K.Wansley E, Camphausen K, Luiten RM, de Ru AH, Neijssen J, et al. Radiation modulates the peptide repertoire, enhances MHC class I expression, and induces successful antitumor immunotherapy. J Exp Med. 2006;203(5):1259–1271. doi:10.1084/jem.20052494.

24. Burnette BC, Liang H, Lee Y, Chlewicki L, Khodarev NN, Weichselbaum RR, Fu Y-X, Auh SL. The efficacy of radiotherapy relies upon induction of type i interferon-dependent innate and adaptive immunity. Cancer Res. 2011;71(7):2488–2496. doi:10.1158/0008-5472.CAN-10-2820.

25. Voorwerk L, Slagter M, Horlings HM, Sikorska K, van de Vijver KK, de Maaker M, Nederlof I, Kluin RJC, Warren S, Ong S, et al. Immune induction strategies in metastatic triple-negative breast cancer to enhance the sensitivity to PD-1 blockade: the TONIC trial. Nat Med. 2019;25(6):920–928. doi:10.1038/s41591-019-0432-4.

26. Kepp O, Senovilla L, Vitale I, Vacchelli E, Adjemian S, Agostinis P, Apetoh L, Aranda F, Barnaba V, Bloy N, et al. Consensus guidelines for the detection of immunogenic cell death. Oncoimmunology. 2014;3(9):e955691-e955691 e955691. doi:10.4161/21624011.2014.955691.

27. Lwin Z-M, Guo C, Salim A, Yip GWC, Chew F-T, Nan J, Thike AA, Tan P-H, Bay B-H. Clinicopathological significance of calreticulin in breast invasive ductal carcinoma. Modern Pathol. 2010;23(12):1559. doi:10.1038/modpathol.2010.173.

28. Dewan MZ, Galloway AE, Kawashima N, Dewyngaert JK, Babb JS, Formenti SC, Demaria S. Fractionated but not single-dose radiotherapy induces an immune-mediated abscopal effect when combined with anti-CTLA-4 antibody. Clini Cancer Res. 2009;15(17):5379–5388. doi:10.1158/1078-0432.CCR-09-0265.

29. Matsumura S, Wang B, Kawashima N, Braunstein S, Badura M, Cameron TO, Babb JS, Schneider RJ, Formenti SC, Dustin ML, et al. Radiation-induced CXCL16 release by breast cancer cells attracts effector T cells. J Immunol. 2008;181(5):3099–3107. doi:10.4049/jimmunol.181.5.3099.

30. Cui L, Her S, Dunne M, Borst GR, De Souza R, Bristow RG, Jaffray DA, Allen C. Significant radiation enhancement effects by gold nanoparticles in combination with cisplatin in triple negative breast cancer cells and tumor xenografts. Radiat Res. 2017;187(2):147–160. doi:10.1667/RR14578.1.

31. den Brok WD, Speers CH, Gondara L, Baxter E, Tyldesley SK, Lohrisch CA. Survival with metastatic breast cancer based on initial presentation, de novo versus relapsed. Breast Cancer Res Treat. 2017;161(3):549–556. doi:10.1007/s10549-016-4080-9.

32. Albanese A, Tang PS, Chan WC. The effect of nanoparticle size, shape, and surface chemistry on biological systems. Annu Rev Biomed Eng. 2012;14:1–16. doi:10.1146/annurev-bioeng-071811-150124.

33. Alkilany AM, Murphy CJ. Toxicity and cellular uptake of gold nanoparticles: what we have learned so far? J Nanoparticle Res. 2010;12(7):2313–2333. doi:10.1007/s11051-010-9911-8.

34. Rossi G, Monticelli L. Gold nanoparticles in model biological membranes: A computational perspective. Biochimica Et Biophysica Acta (BBA) - Biomembranes. 2016;1858(10):2380–2389. doi:10.1016/j.bbamem.2016.04.001.

35. Khlebtsov N, Dykman L. Biodistribution and toxicity of engineered gold nanoparticles: a review of in vitro and in vivo studies. Chem Soc Rev. 2011;40(3):1647–1671. doi:10.1039/C0CS00018C.

36. Beneduci A, Chidichimo G, Tripepi S, Perrotta E. Transmission electron microscopy study of the effects produced by wide-band low-power millimeter waves on MCF-7 human breast cancer cells in culture. Anticancer Res. 2005;25(2a):1009–1013.

37. Galluzzi L, Vitale I, Warren S, Adjemian S, Agostinis P, Martinez AB, Chan TA, Coukos G, Demaria S, Deutsch E, et al.

Consensus guidelines for the definition, detection and interpretation of immunogenic cell death. J Immunother Cancer. 2020;8:1. doi:10.1136/jitc-2019-000337.

38. Anders CK, Carey LA. Biology, metastatic patterns, and treatment of patients with triple-negative breast cancer. Clin Breast Cancer. 2009;9(Suppl 2):S73–81. doi:10.3816/CBC.2009.s.008.

39. Foulkes WD, Smith IE, Reis-Filho JS. Triple-negative breast cancer. N Engl J Med. 2010;363(20):1938–1948. doi:10.1056/NEJMra1001389.

40. Nedeljkovic M, Damjanovic A. Mechanisms of chemotherapy resistance in triple-negative breast cancer-how we can rise to the challenge. Cells. 2019;8:9. doi:10.3390/cells8090957.

41. Eiermann W, Vallis KA. Locoregional treatments for triple-negative breast cancer. Ann Oncol. 2012;23(Suppl 6):vi30–34. doi:10.1093/annonc/mds192.

42. Perrault SD, Walkey C, Jennings T, Fischer HC, Chan WC. Mediating tumor targeting efficiency of nanoparticles through design. Nano Lett. 2009;9(5):1909–1915. doi:10.1021/nl900031y.

43. Dimitriou NM, Tsekenis G, Balanikas EC, Pavlopoulou A, Mitsiogianni M, Mantso T, Pashos G, Boudouvis AG, Lykakis IN, Tsigaridas G, et al. Gold nanoparticles, radiations and the immune system: current insights into the physical mechanisms and the biological interactions of this new alliance towards cancer therapy. Pharmacol Ther. 2017;178:1–17. doi:10.1016/j.pharmthera.2017.03.006.

44. Chithrani BD, Ghazani AA, Chan WC. Determining the size and shape dependence of gold nanoparticle uptake into mammalian cells. Nano Lett. 2006;6(4):662–668. doi:10.1021/nl052396o.

45. Chithrani BD, Chan WCW. Elucidating the mechanism of cellular uptake and removal of protein-coated gold nanoparticles of different sizes and shapes. Nano Lett. 2007;7(6):1542–1550. doi:10.1021/nl070363y.

46. Pan Y, Leifert A, Ruau D, Neuss S, Bornemann J, Schmid G, Brandau W, Simon U, Jahnen-Dechent W. Gold nanoparticles of diameter 1.4 nm trigger necrosis by oxidative stress and mitochondrial damage. Small (Weinheim an Der Bergstrasse, Germany). 2009;5(18):2067–2076. doi:10.1002/smll.200900466.

47. Hvolbæk B, Janssens TVW, Clausen BS, Falsig H, Christensen CH, Nørskov JK. Catalytic activity of Au nanoparticles. Nano Today. 2007;2(4):14–18. doi:10.1016/S1748-0132(07)70113-5.

48. Simpson CA, Huffman BJ, Gerdon AE, Cliffel DE. Unexpected toxicity of monolayer protected gold clusters eliminated by PEG-thiol place exchange reactions. Chem Res Toxicol. 2010;23(10):1608–1616. doi:10.1021/tx100209t.

49. Gilles M, Brun E, Sicard-Roselli C. Gold nanoparticles functionalization notably decreases radiosensitization through hydroxyl radical production under ionizing radiation. Colloids Surf B Biointerfaces. 2014;123:770–777. doi:10.1016/j.colsurfb.2014.10.028.

50. Senut MC, Zhang Y, Liu F, Sen A, Ruden DM, Size-Dependent MG. Toxicity of gold nanoparticles on human embryonic stem cells and their neural derivatives. Small (Weinheim an Der Bergstrasse, Germany). 2016;12(5):631–646. doi:10.1002/smll.201502346.

51. Minic Z, Zhang Y, Mao G, Goshgarian HG. Transporter protein-coupled DPCPX nanoconjugates induce diaphragmatic recovery after SCI by blocking adenosine A1 receptors. J Neurosci. 2016;36(12):3441–3452. doi:10.1523/JNEUROSCI.2577-15.2016.

52. Zhang Y, Walker JB, Minic Z, Liu F, Goshgarian H, Mao G. Transporter protein and drug-conjugated gold nanoparticles capable of bypassing the blood-brain barrier. Sci Rep. 2016;6(1):25794. doi:10.1038/srep25794.

53. Berry CC, de la Fuente JM, Mullin M, Chu SW, Curtis AS. Nuclear localization of HIV-1 tat functionalized gold nanoparticles. IEEE Trans Nanobioscience. 2007;6(4):262–269. doi:10.1109/TNB.2007.908973.

54. Beck M, Forster F, Ecke M, et al. Nuclear pore complex structure and dynamics revealed by cryoelectron tomography. Science. 2004;306(5700):1387–1390. doi:10.1126/science.1104808.

55. Kodiha M, Mahboubi H, Maysinger D, Stochaj U. Gold nanoparticles impinge on nucleoli and the stress response in MCF7 BREAST CANCER CELLS. Nanobiomedicine. 2016;3:3. doi:10.5772/62337.

56. Albanese A, Chan W. Effect of gold nanoparticle aggregation on cell uptake and toxicity. ACS Nano. 2011;5:5478–5489. doi:10.1021/nn2007496.

57. Rizk N, Christoforou N, Lee S. Optimization of anti-cancer drugs and a targeting molecule on multifunctional gold nanoparticles. Nanotechnology. 2016;27(18):185704. doi:10.1088/0957-4484/27/18/185704.

58. Yao X, Huang C, Chen X, Yi Z, Sanche L. Chemical radiosensitivity of DNA induced by gold nanoparticles. J Biomed Nanotechnol. 2015;11(3):478–485. doi:10.1166/jbn.2015.1922.

59. Sia J, Szmyd R, Hau E, Gee HE. Molecular mechanisms of radiation-induced cancer cell death: a primer. Frontiers Cell Dev Bio. 2020;8:41. doi:10.3389/fcell.2020.00041.

60. Chattopadhyay N, Cai Z, Kwon YL, Lechtman E, Pignol JP, Reilly RM. Molecularly targeted gold nanoparticles enhance the radiation response of breast cancer cells and tumor xenografts to X-radiation. Breast Cancer Res Treat. 2013;137(1):81–91. doi:10.1007/s10549-012-2338-4.

61. Zhang X-D, Wu D, Shen X, Chen J, Sun Y-M, Liu P-X, Liang X-J. Size-dependent radiosensitization of PEG-coated gold nanoparticles for cancer radiation therapy. Biomaterials. 2012;33(27):6408–6419. doi:10.1016/j.biomaterials.2012.05.047.

62. Hainfeld JF, Smilowitz HM, O'Connor MJ, Dilmanian FA, Slatkin DN. Gold nanoparticle imaging and radiotherapy of brain tumors in mice. Nanomedicine. 2013;8(10):1601–1609. doi:10.2217/nnm.12.165.

63. Wolfe T, Chatterjee D, Lee J, Grant JD, Bhattarai S, Tailor R, Goodrich G, Nicolucci P, Krishnan S. Targeted gold nanoparticles enhance sensitization of prostate tumors to megavoltage radiation therapy in vivo. Nanomedicine: Nanotechnology, Biology and Medicine. 2015;11(5):1277–1283. doi:10.1016/j.nano.2014.12.016.

64. Herold DM, Das IJ, Stobbe CC, Iyer RV, Chapman JD. Gold microspheres: a selective technique for producing biologically effective dose enhancement. Int J Radiat Biol. 2000;76(10):1357–1364. doi:10.1080/09553000050151637.

65. Chang MY, Shiau AL, Chen YH, Chang CJ, Chen HH, Wu CL. Increased apoptotic potential and dose-enhancing effect of gold nanoparticles in combination with single-dose clinical electron beams on tumor-bearing mice. Cancer Sci. 2008;99(7):1479–1484. doi:10.1111/j.1349-7006.2008.00827.x.

66. Hébert EM, Debouttière P-J, Lepage M, Sanche L, Hunting DJ, Hebert EM, Debouttiere PJ, Lepage M, Sanche L, Hunting DJ. Preferential tumour accumulation of gold nanoparticles, visualised by Magnetic Resonance Imaging: radiosensitisation studies in vivo and in vitro. Int J Radiat Biol. 2010;86(8):692–700. doi:10.3109/09553001003746067.

67. Joh DY, Sun L, Stangl M, Al Zaki A, Murty S, Santoiemma PP, Davis JJ, Baumann BC, Alonso-Basanta M, Bhang D, et al. Selective targeting of brain tumors with gold nanoparticle-induced radiosensitization. PLoS One. 2013;8(4):e62425. doi:10.1371/journal.pone.0062425.

68. De Jong WH, Hagens WI, Krystek P, Burger MC, Sips AJ, Geertsma RE. Particle size-dependent organ distribution of gold nanoparticles after intravenous administration. Biomaterials. 2008;29(12):1912–1919. doi:10.1016/j.biomaterials.2007.12.037.

69. Zhang G, Yang Z, Lu W, Zhang R, Huang Q, Tian M, Li L, Liang D, Li C. Influence of anchoring ligands and particle size on the colloidal stability and in vivo biodistribution of polyethylene glycol-coated gold nanoparticles in tumor-xenografted mice. Biomaterials. 2009;30(10):1928–1936. doi:10.1016/j.biomaterials.2008.12.038.

70. Hainfeld JF, Dilmanian FA, Slatkin DN, Smilowitz HM. Radiotherapy enhancement with gold nanoparticles. J Pharm Pharmacol. 2008;60(8):977–985. doi:10.1211/jpp.60.8.0005.

71. Kim JH, Kolozsvary A, Jenrow KA, Brown SL. Plerixafor, a CXCR4 antagonist, mitigates skin radiation-induced injury in mice. Radiat Res. 2012;178(3):202–206. doi:10.1667/RR2886.1.

72. Charaghvandi RK, Yoo S, van Asselen B, Rodrigues A, van den Bongard D, Horton JK. Treatment constraints for single dose external beam preoperative partial breast irradiation in early-stage breast cancer. Clini Trans Radiat Oncol. 2017;6:7–14. doi:10.1016/j.ctro.2017.06.003.

73. Palta M, Yoo S, Adamson JD, Prosnitz LR, Horton JK. Preoperative single fraction partial breast radiotherapy for early-stage breast cancer. Int J Radiat Oncol Biol Phys. 2012;82(1):37–42. doi:10.1016/j.ijrobp.2010.09.041.

74. Palma DA, Olson R, Harrow S, Gaede S, Louie AV, Haasbeek C, Mulroy L, Lock M, Rodrigues GB, Yaremko BP, et al. Stereotactic ablative radiotherapy versus standard of care palliative treatment in patients with oligometastatic cancers (SABR-COMET): a randomised, phase 2, open-label trial. Lancet. 2019;393 (10185):2051–2058. doi:10.1016/S0140-6736(18)32487-5.

75. Theelen W, Peulen HMU, Lalezari F, van der Noort V, de Vries JF, Aerts JGJV, Dumoulin DW, Bahce I, Niemeijer ALN, de Langen AJ, et al. Effect of pembrolizumab after stereotactic body radiotherapy vs pembrolizumab alone on tumor response in patients with advanced non-small cell lung cancer: results of the PEMBRO-RT phase 2 randomized clinical trial. JAMA oncol. 2019;5:1276. doi:10.1001/jamaoncol.2019.1478.

76. Hall EJ, Giaccia AJ. Radiobiology for the Radiologist. 8 ed. Lippincott Williams & Wilkins (LWW); 2018. ISBN: 978–1–49–633541–8

77. Shultz LD, Goodwin N, Ishikawa F, Hosur V, Lyons BL, Greiner DL. Human cancer growth and therapy in immunodeficient mouse models. Cold Spring Harb Protoc. 2014;2014 (7):694–708. doi:10.1101/pdb.top073585.

78. Kelland LR. Of mice and men: values and liabilities of the athymic nude mouse model in anticancer drug development. European J Cancer (Oxford, England: 1990). 2004;40(6):827–836. doi:10.1016/j.ejca.2003.11.028.

79. Obeid M, Tesniere A, Ghiringhelli F, Fimia GM, Apetoh L, Perfettini J-L, Castedo M, Mignot G, Panaretakis T, Casares N, et al. Calreticulin exposure dictates the immunogenicity of cancer cell death. Nat Med. 2007;13(1):54–61. doi:10.1038/nm1523.

80. Pasparakis M, Vandenabeele P. Necroptosis and its role in inflammation. Nature. 2015;517(7534):311–320. doi:10.1038/nature14191.

81. Eriksson D, Stigbrand T. Radiation-induced cell death mechanisms. Tumour Biol. 2010;31(4):363–372. doi:10.1007/s13277-010-0042-8.

82. McQuaid HN, Muir MF, Taggart LE, McMahon SJ, Coulter JA, Hyland WB, Jain S, Butterworth KT, Schettino G, Prise KM, et al. Imaging and radiation effects of gold nanoparticles in tumour cells.. Scientific Reports. 2016;6:19442. doi:10.1038/srep19442.

83. Ma Y, Kepp O, Ghiringhelli F, Apetoh L, Aymeric L, Locher C, Tesniere A, Martins I, Ly A, Haynes NM, et al. Chemotherapy and radiotherapy: cryptic anticancer vaccines. Semin Immunol. 2010;22(3):113–124. doi:10.1016/j.smim.2010.03.001.

84. Turkevich J, Stevenson PC, Hillier JA, Study of the nucleation and growth processes in the synthesis of. Gold C. Discuss Faraday Soc. 1951;11:55-&. doi:10.1039/df9511100055.

85. Controlled FG. Nucleation for regulation of particle-size in mono-disperse gold suspensions. Nature-Phys Sci. 1973;241(105):20–22. doi:10.1038/physci241020a0.

86. Kimling J, Maier M, Okenve B, Kotaidis V, Ballot H, Plech A. Turkevich method for gold nanoparticle synthesis revisited. J Phys Chem B. 2006;110(32):15700–15707. doi:10.1021/jp061667w.

87. Bankhead P, Loughrey MB, Fernández JA, Dombrowski Y, McArt DG, Dunne PD, McQuaid S, Gray RT, Murray LJ, Coleman HG, et al. QuPath: open source software for digital pathology image analysis. Sci Rep. 2017;7(1):16878. doi:10.1038/s41598-017-17204-5.